THE JOURNAL OF PHYSICAL CHEMISTRY C

Article

Cite This: J. Phys. Chem. C 2018, 122, 17136−17142

pubs.acs.org/JPCC

Mechanism of Efficient Viologen Radical Generation by Ultrafast Electron Transfer from CdS Quantum Dots

Fengjiao Zhao,[†,‡,§] Qiuyang Li,[†] Keli Han,[‡] and Tianquan Lian*[,†]

[†]Department of Chemistry, Emory University, Atlanta, Georgia 30322, United States

[‡]State Key Laboratory of Molecular Reaction Dynamics, Dalian Institute of Chemical Physics, Chinese Academy of Sciences, Dalian 116023, China

[§]University of the Chinese Academy of Sciences, Beijing 100049, China

Supporting Information

ABSTRACT: Artificial photosynthetic systems consisted of nanocrystal light absorbers, molecular redox mediators, and catalysts are one of the most promising and flexible approaches for solar fuel generation because their constituents can be independently tuned. In this work, we investigate the photoreduction of three viologen derivatives, one of the most widely investigated molecular redox mediators, of different redox potentials, 7,8-dihydro-6*H*-dipyrido[1,2-*a*:2′,1′-*c*][1,4]-diazepinediium (PDQ^{2+}), methyl viologen (MV^{2+}), and benzyl viologen (BV^{2+}), using CdS quantum dots (QDs) as the light absorber and mercaptopropionic acid as a sacrificial electron donor in aqueous (pH = 7) solution. Under continuous 405 nm light-emitting diode illumination, the steady-state radical generation quantum yield (QY) follows the order of $PDQ^{\bullet+}$ (15.99%) > $MV^{\bullet+}$ (12.61%) > $BV^{\bullet+}$ (6.56%). Transient absorption spectroscopy studies show that while the rates of initial electron transfer (ET) from the excited QD conduction band to the mediators, following the order of BV^{2+} > MV^{2+} > PDQ^{2+}, decrease for mediators with more negative redox potentials (and lower ET driving force), the initial transient charge separation QYs are unity in all samples because these ET rates are much faster than the intrinsic exciton decay within the QD. The steady-state QYs are much smaller than unity because of charge recombination (CR), whose rates, following the order of BV^{2+} > MV^{2+} > PDQ^{2+}, decrease for mediators with more negative redox potentials (and higher ET driving force in the Marcus' inverted regime). In these systems, there exists a long-lived component in the radial decay kinetics, whose amplitudes determine the steady-state radical generation QYs. We speculate that the desorption of the radical from the QD surface is essential for the suppression of CR and is responsible for the steady-state generation of radicals. This work provides new insight for rational design and improvement of efficient QD/redox mediator-based photoreduction systems.

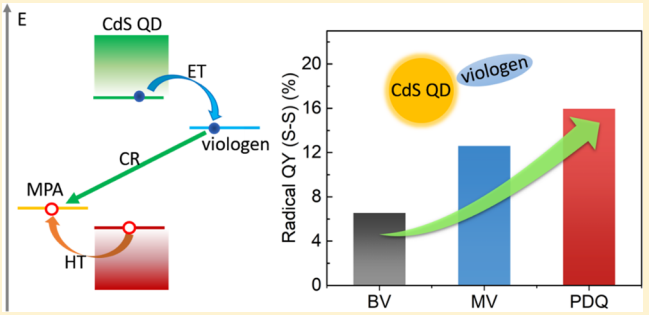

INTRODUCTION

Converting renewable and abundant solar energy into clean chemical fuels through artificial photosynthesis has attracted intensive attentions in recent years.[1−4] Quantum confined semiconductor nanocrystals have shown great potentials as light-harvesting materials in many photosynthetic systems because their optical properties and redox potentials can be tuned by their sizes through the quantum confinement effect and charge recombination (CR) times can be controlled by their morphologies.[4−14] One of the most promising approaches is to use redox mediators to deliver electrons or holes from the light-harvesting component to catalysts to drive the overall photodriven catalytic transformation. Viologens are frequently used as mediators in many light-driven hydrogen generation and CO_2 reduction systems because their redox potentials conveniently fall between the conduction band (CB) edge of the semiconductor materials and the reduction potential of these important fuel-forming reactions.[10−13,15,16] Moreover, viologen radicals are relatively stable in anaerobic conditions and have distinct spectral signatures that enable unambiguous *in situ* spectroscopic studies.[14−18]

Photoreduction of methyl viologens, one of the most common viologen derivatives, by quantum confined nanocrystals has been extensively studied.[15,17−19] This process was shown to depend sensitively on the morphology and composition of the nanocrystals, and a near unity photoreduction quantum yield (QY) has been reported using CdSe@CdS dot-in-rod nanorods. However, it has also been reported that the redox potential of methyl viologens is not sufficiently negative to drive H_2 reduction reaction effectively at pH 7 or higher and the use of viologen derivatives with more negative potentials can significantly improve the overall QY.[15,16] In such artificial photosynthetic systems, the overall reaction is complex and its QY depends on both the QYs of initial radical generation and the subsequent catalytic

Received: July 9, 2018
Published: July 11, 2018

DOI: 10.1021/acs.jpcc.8b06551
J. Phys. Chem. C 2018, 122, 17136−17142

conversion driven by the radical, both of which can be influenced by the redox potentials of the mediators. Therefore, a detailed understanding of both processes is essential for the rational design of such mediator-based photocatalytic systems.

In this paper, we report a study of the photoreduction of viologen derivatives of different redox potentials, 7,8-dihydro-6*H*-dipyrido[1,2-*a*:2′,1′-*c*][1,4]diazepinediium dibromide [PDQ^{2+}, −550 mV vs normal hydrogen electrode (NHE)], methyl viologen (MV^{2+}, −448 mV), and benzyl viologen (BV^{2+}, −370 mV),[20] using CdS quantum dots (QDs) as a photosensitizer and 3-mercaptopropionic acid (MPA) as a sacrificial donor (Figure 1A,B). We show that the steady-state radical generation QY of these radical generation systems increases from BV^{2+}, MV^{2+}, to PDQ^{2+}. To understand how the photoreduction QY depends on their redox potential, we carried out a detailed transient absorption (TA) spectroscopic study of the charge separation (CS) and CR processes. We discuss how the rates and the efficiencies of these processes depend on the redox potentials of the mediator and how these dependences affect the overall steady-state radical generation efficiencies.

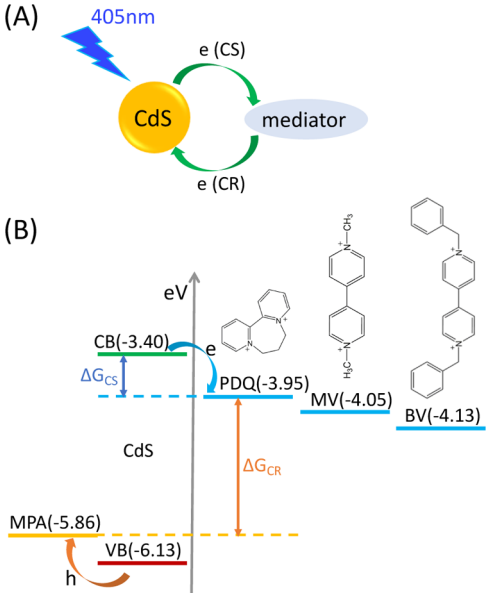

Figure 1. Photodriven processes in QD−viologen complexes. (A) Schematic description of CS and CR processes between CdS QDs and mediators. (B) Redox potentials (vs vacuum) of CdS QD CB and valence band (VB), mediators, and MPA, and schematic molecular structures of PDQ^{2+}, MV^{2+}, and BV^{2+}. ΔG_{CS} and ΔG_{CR} are the driving forces for CS and CR, respectively.

RESULTS AND DISCUSSION

Sample Characterization and Viologen Radical Generation QY. CdS QDs were synthesized following the reported procedures.[21] Their first exciton absorption peak is at 449 nm (Figure S1), which corresponds to an estimated radius of about 2.6 nm.[22] These QDs were rendered water soluble by replacing their native ligands with MPA molecules.[15,23] Synthesis and ligand exchange details are described in the Supporting Information (SI1). We measured the steady-state radical generation QYs of $PDQ^{\bullet+}$, $MV^{\bullet+}$, and $BV^{\bullet+}$ using CdS QDs as a sensitizer at room temperature in a pH = 7 aqueous solution with a phosphate buffer and excess MPA as a sacrificial electron donor under the illumination of 405 nm light-emitting diode (LED) (2.3 mW). All samples were adjusted to the same absorbance at 405 nm [optical density (OD) = 0.3 at 405 nm in 2 mm thick cuvettes] and purged under nitrogen flow for 20 min prior to measurement. Figure 2a shows the absorption spectra of a CdS QD−PDQ sample after different durations of 405 nm illumination. These spectra show a constant first exciton absorption peak of CdS QDs and increased viologen radical absorptions at longer illumination times. To better observe the spectral evolution of the radical, we subtract the spectrum at t = 0 s (containing only QD absorption) from the spectra at later times to produce difference spectra (Figure 2a inset). These difference spectra show both the sharp peak from 320 to 420 nm and broad band from 450 to 580 nm of $PDQ^{\bullet+}$, consistent with literature reports.[24] Similar absorption spectra of other QD−viologen complexes are shown in Figure S3. The amount of generated viologen radicals (N, in moles) is determined from the measured OD of radicals according to the Beer's law: $OD = \varepsilon(N/V)L$, where ε is the extinction coefficients at indicated wavelengths (15 000 M^{-1} cm^{-1} at 383 nm for $PDQ^{\bullet+}$; 13 700 M^{-1} cm^{-1} at 606 nm for $MV^{\bullet+}$; and 17 200 M^{-1} cm^{-1} at 604 nm for $BV^{\bullet+}$),[25−27] V is the sample volume (625 μL), and L is the thickness of the cuvette (2 mm). As shown in Figure 2b, the amount of generated radicals increases with illumination time for all three viologens and is the highest for $PDQ^{\bullet+}$ and lowest for $BV^{\bullet+}$. The radical generation rate for all samples decreases with time. This is likely due to the consumption of MPA and the interference of viologen radicals at the

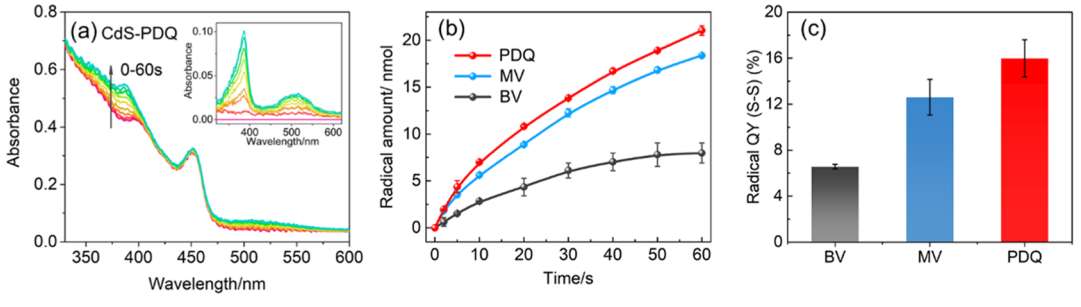

Figure 2. Radical generation in CdS QD−viologen systems. (a) UV−vis absorbance spectra of CdS QDs with PDQ^{2+} after different illumination times (0−60 s in 10 s intervals). Inset: UV−vis difference absorbance spectra (spectrum at time t—spectrum at t = 0) showing the contribution of $PDQ^{\bullet+}$. (b) Amount of generated $PDQ^{\bullet+}$, $MV^{\bullet+}$, and $BV^{\bullet+}$ radicals as a function of illumination time in pH 7 buffer. (c) Viologen radical generation QYs within first 5 s. Experimental conditions: excitation by 405 nm LED light at 2.3 mW; sample OD of 0.3 at 405 nm and in pH 7 aqueous solution with phosphate buffer; and 5 mM mediator concentration.

DOI: 10.1021/acs.jpcc.8b06551
J. Phys. Chem. C 2018, 122, 17136−17142

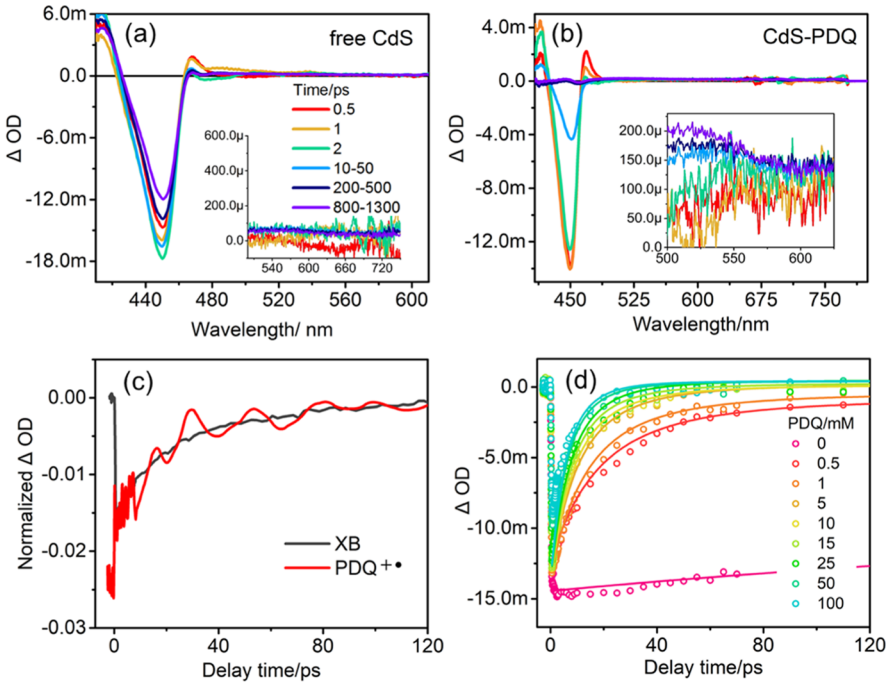

Figure 3. TA spectra and kinetics of CdS QDs with and without PDQ^{2+} in pH = 7 buffer solution with MPA as a sacrificial donor. TA spectra of (a) free CdS QDs and (b) CdS QDs with PDQ (5 mM). Insets: Expanded view of the TA spectra of PDQ radicals at 500−650 nm. (c) Comparison of XB and PDQ radical kinetics. (d) PDQ^{2+} XB kinetics (circles) as a function of PDQ^{2+} concentration (from 0 to 100 mM), and fits (solid lines) according to a model described in the main text.

illumination wavelength. To avoid these effects, the first three points in the radical generation kinetics (0, 2, and 5 s) are used to obtain the initial radical generation rates, from which the radical generation QYs are calculated and shown in Figure 1c.[15] The calculation details are shown in the Supporting Information (SI4).

Ultrafast Electron Transfer from CdS QDs to Viologens. At the excitation wavelength used for steady-state QY measurements (405 nm), the viologen molecules have negligible absorption and their photoreduction occurs by electron transfer (ET) from the excited CdS QDs to viologen lowest unoccupied molecular orbital. As shown in Figure 1B, driving forces for CS, *i.e.*, ET from the QD CB edge (at −3.40 eV vs vacuum) to PDQ^{2+}, MV^{2+}, and BV^{2+} are ∼0.55, ∼0.65, and ∼0.73 eV, respectively.[20,28−34] Details of energy level calculation are shown in the Supporting Information (SI2). The photogenerated radical can undergo CR with the holes in the QD (VB or trapped below the band edge) or oxidized MPA molecules.[35−39] Thus, effective suppression of the CR process is essential for achieving steady-state radical generation.

To understand the observed trend of steady-state radical generation yield, we carried out TA spectroscopy measurements to directly follow the CS and CR processes. We first compare the TA spectra of CdS QDs with and without viologens in pH = 7 buffer with 400 nm excitation (Figure 3a,b). The TA spectra of free CdS QDs (Figure 3a) show a 1S exciton bleach (XB), the negative peak at ∼451 nm. According to our previous studies, XB results from CB edge electron state filling, probing the electron population on 1S CB level.[40−43] Hole state filling contributes negligibly to XB because of the strong degeneracy and mixing between dense hole levels in VB.[15,40,42,43] The TA spectra of CdS QD−PDQ^{2+} complexes (Figure 3b) show that in the presence of PDQ (5 mM), the 1S XB recovers faster than that of free CdS QDs, and the broad PDQ radical ($PDQ^{\bullet+}$) absorption signal appears at 500−575 nm (inset of Figure 3b). As shown in Figure 3c, the decay of XB and the growth of PDQ radical signal agree well with each other, confirming that both can be attributed to ET from excited CdS QDs to viologens. A comparison of the XB kinetics of CdS QD−PDQ complexes with different PDQ concentrations (Figure 3d) shows that XB recovers faster at higher PDQ^{2+} concentrations. The TA spectra, kinetics comparisons, and viologen concentration-dependent XB kinetics of other samples are shown in the Supporting Information (SI5).

To quantify ET rates from CdS QDs to different viologens, we fit the viologen concentration-dependent XB kinetics to a model that is described in the Supporting Information (SI6). This model assumes a Poisson distribution of the number of acceptors on QDs (see eq S4),[44] whose average (m) is related to the solution concentration by the Langmuir adsorption isotherm (SI).[32] It is also assumed that the ET rate increases linearly with the number of acceptors (n) on the QD. The best fits (solid lines in Figure 3d) give the intrinsic ET rates, k_{int}, the ET rate per adsorbed viologen, of 0.21 ± 0.01, 0.13 ± 0.01, and 0.03 ± 0.01 ps^{-1} for BV^{2+}, MV^{2+}, and PDQ^{2+}, respectively (Figure 4a). This reveals that ET from the QD to BV^{2+} molecules is the fastest, followed by MV^{2+}, and then PDQ^{2+}. The transient ET yields are calculated by considering the competition between ET (k_{ET}) and exciton recombination (k_x) (eq S9) as 97.40 ± 0.05, 95.87 ± 0.06, and 84.27 ± 0.16% for BV^{2+}, MV^{2+}, and PDQ^{2+}, respectively (see SI). As shown in Figure 1, the reduction potential becomes less negative from BV^{2+}, MV^{2+}, and PDQ^{2+}, which corresponds to a decreasing driving force for ET from the QD CB edge. Our result suggests that the ET rate from QDs to these viologens increases at

DOI: 10.1021/acs.jpcc.8b06551
J. Phys. Chem. C 2018, 122, 17136−17142

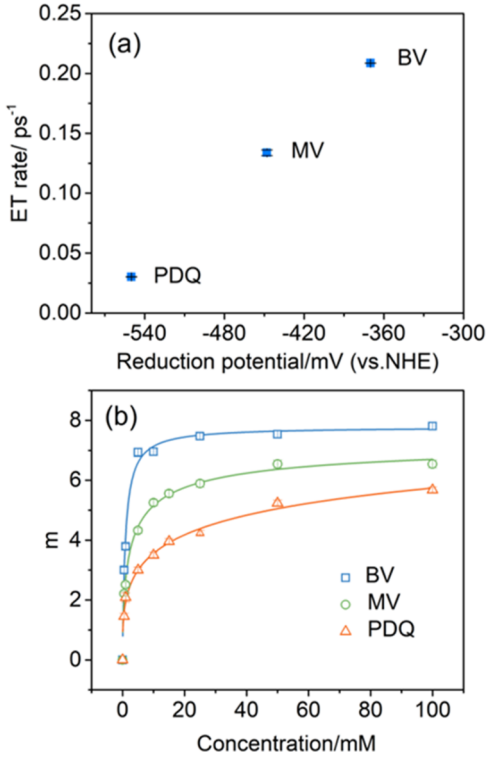

Figure 4. ET rate from QDs to viologens. (a) Intrinsic ET rate (ps^{-1}) as a function of the mediators' reduction potentials (vs NHE); (b) average number of adsorbed mediator molecules on CdS QDs as a function of free mediator concentration in solution; solid lines are fits according to the Langmuir isotherm.

larger driving force, consistent with previously observed trends from similar QDs to methyl viologen and other adsorbates.[32,45]

The best fit also reveals the average number of adsorbed viologens on the QD surface, *m*, as a function of viologen concentration (Figure 4b). With increasing total concentration, the number of viologens adsorbed on QD surfaces first grows at low concentration (<10 mM) and then saturates after 20 mM. The average numbers of adsorbed viologen per QD at saturation (at 100 mM) are 7.81 ± 0.14, 6.54 ± 0.13, and 5.68 ± 0.01 for BV^{2+}, MV^{2+}, and PDQ^{2+}, respectively. At a viologen concentration of 5 mM, which is used in steady-state radical generation measurements, the average number of BV^{2+}, MV^{2+}, and PDQ^{2+} per QD is 6.93 ± 0.14, 4.32 ± 0.09, and 3.00 ± 0.01, respectively (see Table S2). The average number of adsorbates as a function of total viologen concentration can be fit by Langmuir adsorption isotherm (Figure 4b), which yields binding constants, *K*, of 1.12 ± 0.12, 0.65 ± 0.14, and 0.39 ± 0.15 mM^{-1} for BV^{2+}, MV^{2+}, and PDQ^{2+}, respectively (see SI). Because these viologens have the same charge, the difference of their binding constants on the QD surface can likely be attributed to their size and shape, which can affect the strength of their electrostatic interaction with the QD surface ligands.[46]

CR in CdS QD−Viologen Complexes. As shown above, the initial yield for CS is nearly unity for all QD/mediator samples. Thus, the observed steady-state photoreduction yield must be determined by the CR, that is, back transfer of the electron from viologen radicals to the hole in CdS QDs and/or the oxidized hole acceptors (MPA).[35,36]

TA kinetics of the three viologen radical signals are compared in Figure 5, where the initial amplitudes of viologen radical signals (490−520 nm for PDQ, 590−610 nm for MV,

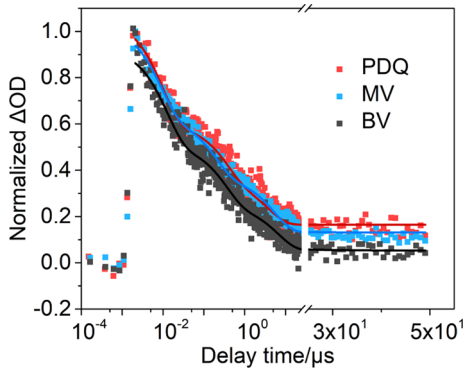

Figure 5. Radical (PDQ, MV, and BV) decay kinetics in pH = 7 phosphate buffer. Dots: raw data; solid lines: fits to triple exponential decay functions.

and 500−550 nm for BV) have been normalized to 1 for comparison. All viologen radical signals show highly nonsingle exponential decay processes: a rapid initial decay (<1 μs) and then much slower change after 20 μs. From the average lifetime (τ_{CR}) of radical decay kinetics calculated by triple-exponential fits (see SI), we calculate the average CR rates ($k_{CR} = 1/\tau_{CR}$) to be 0.29 ± 0.02, 0.19 ± 0.01, and 0.16 ± 0.02 μs^{-1} for $PDQ^{\bullet+}$, $MV^{\bullet+}$, and $BV^{\bullet+}$, respectively (Table 1). Hole transfer from the QD VB to the adsorbed MPA can be measured by time-resolved QD photoluminescence decay, which has been shown to occur on the sub-nanosecond (0.15 ns) time scale in previous studies of similar MPA-capped QDs.[15] Thus, for these QD−viologen complexes, CR is dominated by back ET to the holes localized in the oxidized MPA with CR driving force of 1.91, 1.81, and 1.73 eV for $PDQ^{\bullet+}$, $MV^{\bullet+}$, and $BV^{\bullet+}$, respectively (Figure 1B). The reorganization energy λ for CR consists both inner (λ_i) and outer (λ_o) contributions. On the basis of previous reports, λ_i is estimated to be ∼0.7−1.1 eV for organic molecules of comparable structures[47,48] and λ_o is estimated to be 0.1−0.2 eV for nonpolar solvents.[49] Thus, the total reorganization energy λ is estimated to be ∼0.8−1.3 eV, which is smaller than the CR driving force (ΔG_{CR} in Table 1), indicating that CR falls in the Marcus inverted regime. The measured CR rates increase at smaller driving force, which is consistent with the expected trend of ET in the Marcus inverted regime. The average amplitudes of radical signals at 30−50 μs are ∼15.14 ± 2.81, 11.03 ± 1.52, and 5.13 ± 2.21% for $PDQ^{\bullet+}$, $MV^{\bullet+}$, and $BV^{\bullet+}$, respectively (Table 1), which increases in systems with slower average CR rates. The trend of these transient radical generation QYs at 30−50 μs (QY_T) is consistent with the steady-state QYs (QY_S, Table 1), suggesting that the long-lived radicals are responsible for the steady-state radical yields.

Model for Radical Generation QY. The TA study shows that the rate of the initial CS increases with the driving forces, following the order of BV^{2+} > MV^{2+} > PDQ^{2+}. However, these rates are much faster than the intrinsic electron−hole recombination time within the QDs. As a result, the initial CS yield is near unity for all QD/mediator complexes. The CR rate increases at smaller driving force, following the trend of BV^{2+} > MV^{2+} > PDQ^{2+}, consistent with ET in the Marcus' inverted regime. Although this trend indicates that slower CR correlates with a larger steady-state QY, these average recombination times (on the sub-microsecond time scale) would still suggest a negligible steady-state QY. However, the radical decay kinetics are highly nonsingle exponential,

DOI: 10.1021/acs.jpcc.8b06551
J. Phys. Chem. C 2018, 122, 17136−17142

Table 1. Summary of Results in CS and CR Processes and Radical Generation QYs

	E_0[a] (mV NHE)	ΔG_{CS}[b] (eV)	k_{int}[c] (ps^{-1})	CS yield (%)	ΔG_{CR}[d] (eV)	k_{CR}[e] (μs^{-1})	K[f] (mM^{-1})	QY_S (%)[g]	QY_T (%)[h]
BV^{2+}	−370	0.73	0.21 ± 0.01	97.40 ± 0.05	1.73	0.16 ± 0.02	1.12 ± 0.12	6.56 ± 0.20	5.13 ± 2.21
MV^{2+}	−448	0.65	0.13 ± 0.01	95.87 ± 0.06	1.81	0.19 ± 0.01	0.65 ± 0.14	12.61 ± 1.55	11.03 ± 1.52
PDQ^{2+}	−550	0.55	0.03 ± 0.01	84.27 ± 0.16	1.91	0.29 ± 0.02	0.39 ± 0.15	15.99 ± 1.61	15.14 ± 2.81

[a]E_0: reduction potential. [b]ΔG_{CS}: driving force of CS (from CdS QDs to viologens). [c]k_{int}: intrinsic CS rate. [d]ΔG_{CR}: driving force of CR (ET from viologen radicals to CdS QDs). [e]k_{CR}: average CR rate. [f]K: binding constants of viologens on the CdS QD surface. [g]Radical QY_S: steady-state radical generation QY. [h]QY_T: transient radical generation QY.

showing a long-lived component that decays negligibly on the >1 μs time scale with an amplitude consistent with the steady-state radical generation quantum efficiencies. This suggests that the long-lived component is responsible for steady-state production of viologen radicals in the continuous illumination measurement shown in Figure 2. It is likely that the further removal of the hole (oxidized MPA) and/or the electron (viologen radicals) acceptors from the QD surface occurs on the microsecond time scale. Because this process inhibits CR, the amplitude of the remaining radicals at this time scale (which is determined by the CR rate) determines the steady-state QY. Previous studies have also shown that these radicals, generated initially on the QD surface, can diffuse to Pt particles or hydrogenase to drive H_2 generation.[15,16] It is also important to note that these positively charged viologens bind through electrostatic interaction with negatively charged QD surface (deprotonation of the MPA ligand with a reported pK_a of ∼7 on similar QDs) at pH ≈ 7.[50,51] The reduction of the viologen decreases their positive charge and reduces their binding strength, which facilitates their desorption. Thus, the process of further removal of the electron from the QD surface likely occurs through the desorption of viologen radicals. Interestingly, the observed trend of steady-state radical generation QYs correlates with the binding constants of these viologens on the QD surface, showing a larger steady-state QY in viologens with weaker binding constant. Although these results suggest that viologen radical desorption from the QD surface plays a critical role in preventing CR and achieving steady-state radical generation, further studies are needed to more firmly establish this mechanism.

CONCLUSIONS

We have studied the mechanism of photoreduction of three viologens with increasingly negative reduction potentials (BV^{2+}, MV^{2+}, and PDQ^{2+}) using CdS QDs as the photosensitizer and MPA as the electron donor in aqueous solution. The steady-state measurement shows that the radical generation QYs increase from 6.56 ± 0.20 in BV^{2+} to 12.61 ± 1.55 in MV^{2+} and 15.99 ± 1.61 in PDQ^{2+}. To understand the origin of the observed trend of steady-state QYs, we directly probed the CS and CR processes in QD−viologen complexes by TA spectroscopy. We show that although initial CS rates increase with the ET driving force, following the trend of BV^{2+} > MV^{2+} > PDQ^{2+}, the QYs for this process are near unity for all viologens because the CS rates are much faster than the intrinsic exciton decay rates within the QDs. The CR process is highly none single exponential in these complexes, and the average CR rates increase in complexes with the smaller driving force, following the trend of BV^{2+} > MV^{2+} > PDQ^{2+}, consistent with ET in the Marcus inverted regime. The radical decay kinetics show a long-lived component with negligible decay in the 1−50 μs time scale. The relative amplitude of this component follows the steady QY, indicating that this component is responsible for the steady-state generation of radicals in these systems. This result suggests that the amplitude of this long-lived component is determined by the competition of CR with radical desorption from the QD surface, which inhibits the CR. Our results offer new insight into the rational design of QD/mediator-based systems with improved photoreduction QYs.

ASSOCIATED CONTENT

Supporting Information

The Supporting Information is available free of charge on the ACS Publications website at DOI: 10.1021/acs.jpcc.8b06551.

Synthesis methods, energy level evaluation, steady-state UV−vis absorbance spectra of CdS QD−viologen complexes, radical QY calculation, TA spectra and XB kinetics, fitting details of free CdS QD XB recovery kinetics, Langmuir adsorption isotherm, and ET yields (PDF)

AUTHOR INFORMATION

Corresponding Author

*E-mail: tlian@emory.edu.

ORCID

Fengjiao Zhao: 0000-0001-8691-0889

Keli Han: 0000-0001-9239-1827

Tianquan Lian: 0000-0002-8351-3690

Notes

The authors declare no competing financial interest.

ACKNOWLEDGMENTS

This material is based upon the work supported by the U.S. Department of Energy, Office of Science, Office of Basic Energy Sciences, Solar Photochemistry Program under award number (DE-FG02-12ER16347). F.Z. acknowledges the support from the National Key Research and Development Program of China (grant 2017YFA0204800), the National Natural Science Foundation of China (grant no. 21533010), and financial support from the China Scholarship Council.

REFERENCES

(1) Gray, H. B. Powering the Planet with Solar Fuel. *Nat. Chem.* **2009**, *1*, 7.

(2) Grätzel, M. Photoelectrochemical Cells. *Nature* **2001**, *414*, 338−344.

(3) Walter, M. G.; Warren, E. L.; McKone, J. R.; Boettcher, S. W.; Mi, Q.; Santori, E. A.; Lewis, N. S. Solar Water Splitting Cells. *Chem. Rev.* **2010**, *110*, 6446−6473.

(4) Chen, X.; Li, C.; Grätzel, M.; Kostecki, R.; Mao, S. S. Nanomaterials for Renewable Energy Production and Storage. *Chem. Soc. Rev.* **2012**, *41*, 7909−7937.

(5) Talapin, D. V.; Lee, J.-S.; Kovalenko, M. V.; Shevchenko, E. V. Prospects of Colloidal Nanocrystals for Electronic and Optoelectronic Applications. *Chem. Rev.* **2010**, *110*, 389−458.

DOI: 10.1021/acs.jpcc.8b06551
J. Phys. Chem. C 2018, 122, 17136−17142

(6) Zhu, H.; Lian, T. Wavefunction Engineering in Quantum Confined Semiconductor Nanoheterostructures for Efficient Charge Separation and Solar Energy Conversion. *Energy Environ. Sci.* **2012**, *5*, 9406−9418.
(7) Wu, K.; Zhu, H.; Lian, T. Ultrafast Exciton Dynamics and Light-Driven H2 Evolution in Colloidal Semiconductor Nanorods and Pt-Tipped Nanorods. *Acc. Chem. Res.* **2015**, *48*, 851−859.
(8) Wu, K.; Lian, T. Quantum Confined Colloidal Nanorod Heterostructures for Solar-to-Fuel Conversion. *Chem. Soc. Rev.* **2016**, *45*, 3781−3810.
(9) Xie, G.; Zhang, K.; Guo, B.; Liu, Q.; Fang, L.; Gong, J. R. Graphene-Based Materials for Hydrogen Generation from Light-Driven Water Splitting. *Adv. Mater.* **2013**, *25*, 3820−3839.
(10) Li, Q.; Meng, H.; Zhou, P.; Zheng, Y.; Wang, J.; Yu, J.; Gong, J. Zn1-xCdxS Solid Solutions with Controlled Bandgap and Enhanced Visible-Light Photocatalytic H2-Production Activity. *ACS Catal.* **2013**, *3*, 882−889.
(11) Zhang, J.; Yu, J.; Jaroniec, M.; Gong, J. R. Noble Metal-Free Reduced Graphene Oxide-ZnxCd1-xS Nanocomposite with Enhanced Solar Photocatalytic H2-Production Performance. *Nano Lett.* **2012**, *12*, 4584−4589.
(12) Zhang, J.; Yu, J.; Zhang, Y.; Li, Q.; Gong, J. R. Visible Light Photocatalytic H2-Production Activity of Cus/Zns Porous Nanosheets Based on Photoinduced Interfacial Charge Transfer. *Nano Lett.* **2011**, *11*, 4774−4779.
(13) Li, Q.; Guo, B.; Yu, J.; Ran, J.; Zhang, B.; Yan, H.; Gong, J. R. Highly Efficient Visible-Light-Driven Photocatalytic Hydrogen Production of Cds-Cluster-Decorated Graphene Nanosheets. *J. Am. Chem. Soc.* **2011**, *133*, 10878−10884.
(14) Zhang, K.; Dai, Y.; Zhou, Z.; Ullah Jan, S.; Guo, L.; Gong, J. R. Polarization-Induced Saw-Tooth-Like Potential Distribution in Zincblende-Wurtzite Superlattice for Efficient Charge Separation. *Nano Energy* **2017**, *41*, 101−108.
(15) Zhu, H.; Song, N.; Lv, H.; Hill, C. L.; Lian, T. Near Unity Quantum Yield of Light-Driven Redox Mediator Reduction and Efficient H2 Generation Using Colloidal Nanorod Heterostructures. *J. Am. Chem. Soc.* **2012**, *134*, 11701−11708.
(16) Chica, B.; Wu, C.-H.; Liu, Y.; Adams, M. W. W.; Lian, T.; Dyer, R. B. Balancing Electron Transfer Rate and Driving Force for Efficient Photocatalytic Hydrogen Production in Cdse/Cds Nanorod-[Nife] Hydrogenase Assemblies. *Energy Environ. Sci.* **2017**, *10*, 2245−2255.
(17) Dworak, L.; Matylitsky, V. V.; Breus, V. V.; Braun, M.; Basché, T.; Wachtveitl, J. Ultrafast Charge Separation at the Cdse/Cds Core/Shell Quantum Dot/Methylviologen Interface: Implications for Nanocrystal Solar Cells. *J. Phys. Chem. C* **2011**, *115*, 3949−3955.
(18) Wu, K.; Li, Q.; Du, Y.; Chen, Z.; Lian, T. Ultrafast Exciton Quenching by Energy and Electron Transfer in Colloidal Cdse Nanosheet-Pt Heterostructures. *Chem. Sci.* **2015**, *6*, 1049−1054.
(19) Okuhata, T.; Tamai, N. Face-Dependent Electron Transfer in Cdse Nanoplatelet−Methyl Viologen Complexes. *J. Phys. Chem. C* **2016**, *120*, 17052−17059.
(20) Wardman, P. Reduction Potentials of One-Electron Couples Involving Free Radicals in Aqueous Solution. *J. Phys. Chem. Ref. Data* **1989**, *18*, 1637−1755.
(21) Yu, W. W.; Peng, X. Formation of High-Quality CdS and Other II-VI Semiconductor Nanocrystals in Noncoordinating Solvents: Tunable Reactivity of Monomers. *Angew. Chem., Int. Ed.* **2002**, *41*, 2368−2371.
(22) Yu, W. W.; Qu, L.; Guo, W.; Peng, X. Experimental Determination of the Extinction Coefficient of Cdte, Cdse, and Cds Nanocrystals. *Chem. Mater.* **2003**, *15*, 2854−2860.
(23) Wu, K.; Chen, Z.; Lv, H.; Zhu, H.; Hill, C. L.; Lian, T. Hole Removal Rate Limits Photodriven H2 Generation Efficiency in CdS-Pt and CdSe/CdS-Pt Semiconductor Nanorod-Metal Tip Heterostructures. *J. Am. Chem. Soc.* **2014**, *136*, 7708−7716.
(24) Farrington, J. A.; Ebert, M.; Land, E. J. Bipyridylium Quaternary Salts and Related Compounds. Part 6.-Pulse Radiolysis Studies of the Reaction of Paraquat Radical Analogues with Oxygen. *J. Chem. Soc., Faraday Trans. 1* **1978**, *74*, 665.
(25) Tsukahara, K.; Wilkins, R. G. Kinetics of Reduction of Eight Viologens by Dithionite Ion. *J. Am. Chem. Soc.* **1985**, *107*, 2632−2635.
(26) Watanabe, T.; Honda, K. Measurement of the Extinction Coefficient of the Methyl Viologen Cation Radical and the Efficiency of Its Formation by Semiconductor Photocatalysis. *J. Phys. Chem.* **1982**, *86*, 2617−2619.
(27) Mayhew, S. G.; Müller, F. *Dimerization of the Radical Cation of Benzyl Viologen in Aqueous Solution*; Portland Press Limited, 1982.
(28) Bawendi, M.; Steigerwald, M. L.; Brus, L. E. The Quantum Mechanics of Larger Semiconductor Clusters ("Quantum Dots"). *Annu. Rev. Phys. Chem.* **1990**, *41*, 477−496.
(29) Steigerwald, M. L.; Brus, L. E. Semiconductor Crystallites: A Class of Large Molecules. *Acc. Chem. Res.* **1990**, *23*, 183−188.
(30) Brus, L. E. A Simple Model for the Ionization Potential, Electron Affinity, and Aqueous Redox Potentials of Small Semiconductor Crystallites. *J. Chem. Phys.* **1983**, *79*, 5566−5571.
(31) Li, Q.; Wu, K.; Chen, J.; Chen, Z.; McBride, J. R.; Lian, T. Size-Independent Exciton Localization Efficiency in Colloidal Cdse/Cds Core/Crown Nanosheet Type-I Heterostructures. *ACS Nano* **2016**, *10*, 3843−3851.
(32) Zhu, H.; Yang, Y.; Hyeon-Deuk, K.; Califano, M.; Song, N.; Wang, Y.; Zhang, W.; Prezhdo, O. V.; Lian, T. Auger-Assisted Electron Transfer from Photoexcited Semiconductor Quantum Dots. *Nano Lett.* **2014**, *14*, 1263−1269.
(33) Zacharoff, L.; Chan, C. H.; Bond, D. R. Reduction of Low Potential Electron Acceptors Requires the Cbcl Inner Membrane Cytochrome of Geobacter Sulfurreducens. *Bioelectrochemistry* **2016**, *107*, 7−13.
(34) Xu, Y.; Schoonen, M. A. A. The absolute energy positions of conduction and valence bands of selected semiconducting minerals. *Am. Mineral.* **2000**, *85*, 543−556.
(35) Zhu, H.; Song, N.; Rodríguez-Córdoba, W.; Lian, T. Wave Function Engineering for Efficient Extraction of up to Nineteen Electrons from One Cdse/Cds Quasi-Type Ii Quantum Dot. *J. Am. Chem. Soc.* **2012**, *134*, 4250−4257.
(36) Scholz, F.; Dworak, L.; Matylitsky, V. V.; Wachtveitl, J. Ultrafast Electron Transfer from Photoexcited Cdse Quantum Dots to Methylviologen. *ChemPhysChem* **2011**, *12*, 2255−2259.
(37) Maniga, N. I.; Sumida, J. P.; Stone, S.; Moore, A. L.; Moore, T. A.; Gust, D. Increasing the Yield of Photoinduced Charge Separation through Parallel Electron Transfer Pathways. *J. Porphyrins Phthalocyanines* **1999**, *03*, 32−44.
(38) Zhang, Y.; Dood, J.; Beckstead, A. A.; Li, X.-B.; Nguyen, K. V.; Burrows, C. J.; Improta, R.; Kohler, B. Efficient Uv-Induced Charge Separation and Recombination in an 8-Oxoguanine-Containing Dinucleotide. *Proc. Natl. Acad. Sci. U.S.A.* **2014**, *111*, 11612−11617.
(39) Kawai, K.; Majima, T. Photoinduced Charge-Separation in DNA. *Photoinduced Phenomena in Nucleic Acids II*; Springer, 2014; pp 165−182.
(40) Huang, J.; Stockwell, D.; Huang, Z.; Mohler, D. L.; Lian, T. Photoinduced Ultrafast Electron Transfer from Cdse Quantum Dots to Re-Bipyridyl Complexes. *J. Am. Chem. Soc.* **2008**, *130*, 5632−5633.
(41) Wu, K.; Liu, Z.; Zhu, H.; Lian, T. Exciton Annihilation and Dissociation Dynamics in Group II-V Cd3P2 Quantum Dots. *J. Phys. Chem. A* **2013**, *117*, 6362−6372.
(42) Wu, K.; Liang, G.; Kong, D.; Chen, J.; Chen, Z.; Shan, X.; McBride, J. R.; Lian, T. Quasi-type II CuInS2/CdS core/shell quantum dots. *Chem. Sci.* **2016**, *7*, 1238−1244.
(43) Chen, J.; Wu, K.; Rudshteyn, B.; Jia, Y.; Ding, W.; Xie, Z.-X.; Batista, V. S.; Lian, T. Ultrafast Photoinduced Interfacial Proton Coupled Electron Transfer from CdSe Quantum Dots to 4,4′-Bipyridine. *J. Am. Chem. Soc.* **2016**, *138*, 884−892.
(44) Morris-Cohen, A. J.; Frederick, M. T.; Cass, L. C.; Weiss, E. A. Simultaneous Determination of the Adsorption Constant and the Photoinduced Electron Transfer Rate for a Cds Quantum Dot-Viologen Complex. *J. Am. Chem. Soc.* **2011**, *133*, 10146−10154.
(45) Olshansky, J. H.; Ding, T. X.; Lee, Y. V.; Leone, S. R.; Alivisatos, A. P. Hole Transfer from Photoexcited Quantum Dots:

DOI: 10.1021/acs.jpcc.8b06551
J. Phys. Chem. C 2018, 122, 17136−17142

The Relationship between Driving Force and Rate. *J. Am. Chem. Soc.* **2015**, *137*, 15567−15575.
(46) Peterson, M. D.; Jensen, S. C.; Weinberg, D. J.; Weiss, E. A. Mechanisms for Adsorption of Methyl Viologen on Cds Quantum Dots. *ACS Nano* **2014**, *8*, 2826−2837.
(47) Gruhn, N. E.; Macías-Ruvalcaba, N. A.; Evans, D. H. Studies of the Inner Reorganization Energies of the Cation Radicals of 1,4-Bis(Dimethylamino)Benzene, 9,10-Bis(Dimethylamino)Anthracene, and 3,6-Bis(Dimethylamino)Durene by Photoelectron Spectroscopy and Reinterpretation of the Mechanism of the Electrochemical Oxidation of the Parent Diamines. *J. Phys. Chem. A* **2006**, *110*, 5650−5655.
(48) Li, X.-Y.; Tong, J.; He, F.-C. Ab initio calculation for inner reorganization energy of gas-phase electron transfer in organic molecule-ion systems. *Chem. Phys.* **2000**, *260*, 283−294.
(49) Zimmt, M. B.; Waldeck, D. H. Exposing Solvent's Roles in Electron Transfer Reactions: Tunneling Pathway and Solvation. *J. Phys. Chem. A* **2003**, *107*, 3580−3597.
(50) Voráčová, I.; Klepárník, K.; Lišková, M.; Foret, F. Determination of ζ-Potential, Charge, and Number of Organic Ligands on the Surface of Water Soluble Quantum Dots by Capillary Electrophoresis. *Electrophoresis* **2015**, *36*, 867−874.
(51) Burris, S. C.; Zhou, Y.; Maupin, W. A.; Ebelhar, A. J.; Daugherty, M. W. The Effect of Surface Preparation on Apparent Surface pKa's of ω-Mercaptocarboxylic Acid Self-Assembled Monolayers on Polycrystalline Gold. *J. Phys. Chem. C* **2008**, *112*, 6811−6815.

DOI: 10.1021/acs.jpcc.8b06551
J. Phys. Chem. C 2018, 122, 17136−17142